AGU PUBLICATIONS

Radio Science

RESEARCH ARTICLE
10.1002/2016RS006093

New capabilities of the upgraded EISCAT high-power HF facility

M. T. Rietveld[1,2], A. Senior[3], J. Markkanen[4,5], and A. Westman[6]

[1]EISCAT Scientific Association, Ramfjordbotn, Norway, [2]Department of Physics and Technology, University of Tromsø - The Arctic University of Norway, Tromsø, Norway, [3]Formerly at Department of Physics, Lancaster University, Lancaster, UK, [4]EISCAT Scientific Association, Sodankylä, Finland, [5]Sodankylä Geophysical Observatory, University of Oulu, Oulu, Finland, [6]EISCAT Scientific Association, Kiruna, Sweden

Key Points:
- The EISCAT ionospheric heating facility near Tromsø, Norway, has been upgraded in recent years
- A high-power HF radar mode has been implemented to investigate the mesosphere and magnetosphere
- Fast frequency stepping is routinely done with interesting results

Correspondence to:
M. T. Rietveld,
mike.rietveld@eiscat.uit.no

Citation:
Rietveld, M. T., A. Senior, J. Markkanen, and A. Westman (2016), New capabilities of the upgraded EISCAT high-power HF facility, *Radio Sci.*, *51*, doi:10.1002/2016RS006093.

Received 26 MAY 2016
Accepted 19 AUG 2016
Accepted article online 23 AUG 2016

Abstract The high-power HF (high-frequency) facility (commonly known as Heating) near Tromsø, Norway, which is an essential part of the European Incoherent Scatter Scientific Association, has been upgraded in certain key areas in recent years. It is one of only four similar facilities in the world operating at present. An updated description of the facility is given, together with scientific motivation and some results. The main high-power parts such as transmitters, feed-system, and antennas remain essentially the same as built in the late 1970s. The improvements are in the areas of radio frequency waveform generation, computer control, and monitoring. In particular, fast stepping in frequency is now possible, an important aspect in examining features close to harmonics of the electron gyrofrequency. One antenna array has been modified to allow reception to implement an HF radar mode for mesospheric and magnetospheric probing. More realistic modeling of the antenna gain gives improved estimates of the total effective radiated power for both wanted and unwanted circular polarizations. Results are presented by using these new capabilities, but their full scientific potential has yet to be achieved.

1. Introduction

The last three decades have seen major advances in using powerful radio waves injected into the ionosphere to learn about plasma physical processes as well as about the ionosphere and upper atmosphere. There are presently only four known active facilities of this type around the world. They are in chronological order, Sura in Russia [*Belikovich et al.*, 2007], European Incoherent Scatter's (EISCAT's) "Heating" facility (built and formerly run by Germany's Max Planck Institute), High Frequency Active Auroral Research Program (HAARP) [*Pedersen and Carlson*, 2001] in Alaska, and most recently a new HF facility for the Arecibo 300 m antenna, which has just come online. Apart from Arecibo, the EISCAT HF facility is the only one co-located with an incoherent scatter radar (ISR), although HAARP has a small phased array radar which can receive HF-enhanced echoes normally seen with incoherent scatter radars. Indeed, the powerful EISCAT HF facility is co-located with two ISRs at 224 MHz and 930 MHz as well as a 56 MHz mesosphere-stratosphere-troposphere (MST) radar. It is also situated in a region with a wealth of other diagnostic instruments for monitoring the ionosphere and upper atmosphere, making it unique and in high demand for experiments. The EISCAT HF facility has been described in reasonable detail in two publications and a report more than 20 years ago [*Stubbe and Kopka*, 1979; *Stubbe et al.*, 1982; *Rietveld et al.*, 1993]. Since then, advances in electronics and computing have resulted in significant improvements in the control, monitoring, and parameterization of the radiated beam allowing more flexible operation for a wider range of scientific experiments. Furthermore, an HF radar mode has been introduced to give a unique high-power large-aperture radar. These improvements warrant an updated description of the facility, which is expected to continue operation into the near future.

2. Overview of Scientific Results Utilizing Powerful HF Waves at EISCAT

As of August 2016 a total of 395 publications have come out of the heating facility and 272 of these since 1993 when it was transferred from the Max Planck Society to the EISCAT Scientific Association. The list of publications is available at http://www.eiscat.se/groups/Documentation/Publications/Heatingpubs.html. We point out some of the major areas of research that are being addressed currently and which have influenced and are still driving further upgrades of the facility.

One major area of investigation has been plasma physics, where the ionosphere is used as a plasma laboratory to study plasma instabilities, artificially induced plasma turbulence, and their effects such as the generation of accelerated electrons, irregularities, and electron heating. Incoherent scatter radars provide one of the best diagnostics to study the plasma waves excited by the HF pump [e.g., *Rietveld et al*., 2000]. *Kosch et al*. [2007] give a recent review of the thermospheric optical emissions from RF heating. An important early discovery made by using the Tromsø heater was that relatively simple HF measurements on the ground of the reflected HF wave showed a rich set of sidebands both upshifted and downshifted from the HF pump frequency produced by plasma instabilities in the ionosphere [*Thidé et al*., 1982; *Stubbe et al*., 1984]. The phenomenon, called stimulated electromagnetic emission or SEE, is still the subject of an extensive area of research and is reviewed by *Leyser* [2001].

A major discovery made in the 1980s showed that very many effects depend in their strength and nature on how close the pump frequency is to a harmonic of the electron gyrofrequency at the height of interaction [e.g., *Leyser et al*., 1989]. In order to perform such experiments it is highly desirable to change HF rapidly either as a continuous sweep or in many small steps. Frequency stepping was a slow and tedious procedure with the facility up to about 2009; hence, it was one of the major driving forces for an upgraded RF-generation system.

Another significant discovery was the fact that several HF-induced phenomena in the *F* region are especially strong when pumping in the magnetic field-aligned direction. For example, the optical emissions [*Kosch et al*., 2000, 2014], electron heating [*Rietveld et al*., 2003, 2004], and ion upwelling [*Kosch et al*., 2010] all are strongest when the HF beam is pointed along the magnetic field. The discovery of artificial ionization in recent years, which at HAARP has been detected as artificial layers, is discussed in detail by *Mishin et al*. [2016] and references therein.

Most of the experiments investigating plasma instabilities, such as parametric decay near the HF reflection height and upper hybrid resonance slightly below the reflection height, have used ordinary (O) or right-hand circularly polarized mode. This is because the extraordinary (X) mode is reflected before reaching these heights, but in recent years some X-mode effects have been discovered that are not easily explainable [e.g., *Blagoveshchenskaya et al*., 2015]. This, together with the rather mysterious ISR backscatter enhancements extending well above the HF reflection altitude [*Senior et al*., 2013] which also appear to be generated preferentially by X-mode pumping, has driven the requirement to be able to quickly change HF polarization and power level and to determine more precisely the transmitted power and beam shape for both wanted and unwanted polarizations. These improved capabilities are described later.

The HF facility has increasingly been used to learn about the environment of the upper atmosphere. One example is the deduction of neutral atmospheric composition [*Kalogerakis et al*., 2009] from the time constant of the decay of the artificially excited 630 nm red line of oxygen. *Kosch et al*. [2010] used HF pump-induced ion upwelling as measured by the EISCAT UHF radar to show that it should be possible to estimate the *F* layer ion-neutral collision frequency and neutral density with altitude from such ground-based observations.

Leyser and Wong [2009] reviewed ways that powerful HF waves can give us information about the geospace environment as well as ways that they can influence the environment in a very broad sense. A unique application of such HF facilities is the use of artificial periodic irregularities (API) to study the ionosphere and upper atmosphere, a technique pioneered at the Russian Sura facility [*Belikovich et al*., 2007]. This has been implemented at EISCAT in the 1990s [*Rietveld et al*., 1996; *Rietveld and Goncharov*, 1998] using the HF facility as a transmitter and the Dynasonde as a receiver. Some new results from this technique with the upgraded facility are given by *Vierinen et al*. [2013], where one of the heater antenna arrays is used as a receiving antenna.

Mesospheric investigations with the HF facility have been vigorously pursued ever since the discovery that electron temperature increases in the *D* region can weaken [*Chilson et al*., 2000] and strengthen [*Havnes et al*., 2003] polar mesospheric echoes. Modeling [e.g., *Mahmoudian et al*., 2011; *Biebricher and Havnes*, 2012] predicts that the relative importance of charging of mesospheric dust versus electron diffusion on the echo strength increases with the radar wavelength, and recent work has concentrated on using up to four different wavelength radars to compare the measured suppression and overshoot phenomena with these predictions [e.g., *Senior et al*., 2014].

3. Review of HF Facility Specifications

In this section we summarize the main technical parameters of the EISCAT HF facility since early 2012. Earlier descriptions by *Stubbe and Kopka* [1979], *Stubbe et al*. [1982], and *Rietveld et al*. [1993] are thereby updated.

Major changes have been made in the RF generation hardware and in the software used to monitor and control the facility. A radar capability has also been introduced, which never existed before.

The transmitters have not changed at all since they were completed in 1980. There are 12 transmitters of ~100 kW continuous power capable of covering the range of 2.7 to 8.0 MHz but the present antennas only allow the use of frequencies between 3.85 and 8 MHz. Aging of the transmitter tubes means that 80 kW is the normally used maximum power per transmitter in recent years. New tubes are no longer available, and rebuilding of old tubes has had very limited success. Each transmitter has a tetrode vacuum tube operated in class AB as the main amplifier, which is driven by a wideband transistor driver. Both of these are water-cooled. Each transmitter has its own high-voltage power supply delivering up to 12 kV, which is connected directly to the mains supply.

The quasi-linear class AB operation results in about one third of the full power consumption being used by the DC quiescent current when the high voltage is on but no RF is being radiated. In 1997, a power-saving measure was introduced whereby the control grid bias voltage in RF-off intervals longer than about 1 s was switched to a more negative value such that the quiescent current in the transmitting tubes was reduced from about 6 A to about 1.5 A. This switching of the bias voltage of each individual transmitter via relays is now controlled in pairs from the receiver radar-controller in the control room. With a high voltage of 10 kV this amounts to a saving of 45 kW per transmitter or 540 kW in total. In most heating experiments the RF is off for about half the time such that saving 0.5 MW compared to an RF-on power consumption of ~1.7 MW results in significant power cost savings. This is most beneficial because the power used during any 1 h determines the line charges for that month.

In addition to the power saving achieved by changing the control grid bias voltage, the high-voltage relays are now under computer control such that additional power savings can be programmed for RF-off intervals longer than a few minutes. Indeed, the whole HF facility can now be operated under computer control: from cooling pump to filaments, drivers, and high voltage.

The three antenna arrays and transmission line system are exactly the same as described in Figures 2 and 3 of *Rietveld et al*. [1993], which show the electrical details. We give an updated version of the antenna layout and HF facility infrastructure in Figure 1, which also shows the neighboring radars mentioned in this paper. Figure 2 shows in greater detail the exact relationship between the transmitters and their antennas in the various arrays.

The phases at the antennas in each east-west row are fixed by the coaxial cable lengths between the antennas and are set for a vertical radiation pattern. By varying the transmitter phases, one can change the phase between adjacent rows in Array 2 (3.85–5.6 MHz) and Array 3 (5.4–8.0 MHz) to allow steering of the beam in the north-south (geographic) plane out to about ±30° from vertical. In Array 1 (also 5.4–8.0 MHz since 1990) adjacent pairs of antenna rows are connected to one transmitter, which limits the beam steering to about ±20° from vertical, the exact angle depending on frequency. Near these limits grating sidelobes become strong.

An important part of the HF facility is an HF sounder, or ionosonde, which gives real-time information on the state of the ionosphere so that one can decide what HF heating parameters to use. The HF facility has always had its own HF sounder of type Dynasonde, which has also been upgraded in several stages since it started operations in 1980 [*Rietveld et al*., 2008]. The sounder is located in the HF control room building with the transmitting antenna and small receiving array indicated in Figure 1. It has been operating with a 2 min sounding mode since early 2012 to give fast, detailed measurements of the ionosphere. There is also a Digisonde operated by Tromsø Geophysical Observatory on the same site.

4. RF Synthesizers and New Transmission Capabilities

The original 12 HP3325A synthesizers, which were in the control room 300 m from the transmitters, were replaced in 2009 by a new exciter incorporating direct digital synthesis (DDS) units of type AD9953. One major shortcoming of the HP synthesizers was that the initial phase was always random after any frequency change. The phases then had to be measured, compared with what they should be and then changed in an automated procedure, which took at best about 2 min to bring the transmitters to full power for any change in frequency, no matter how small. With the new exciter the phases can be set to any desired value. Other

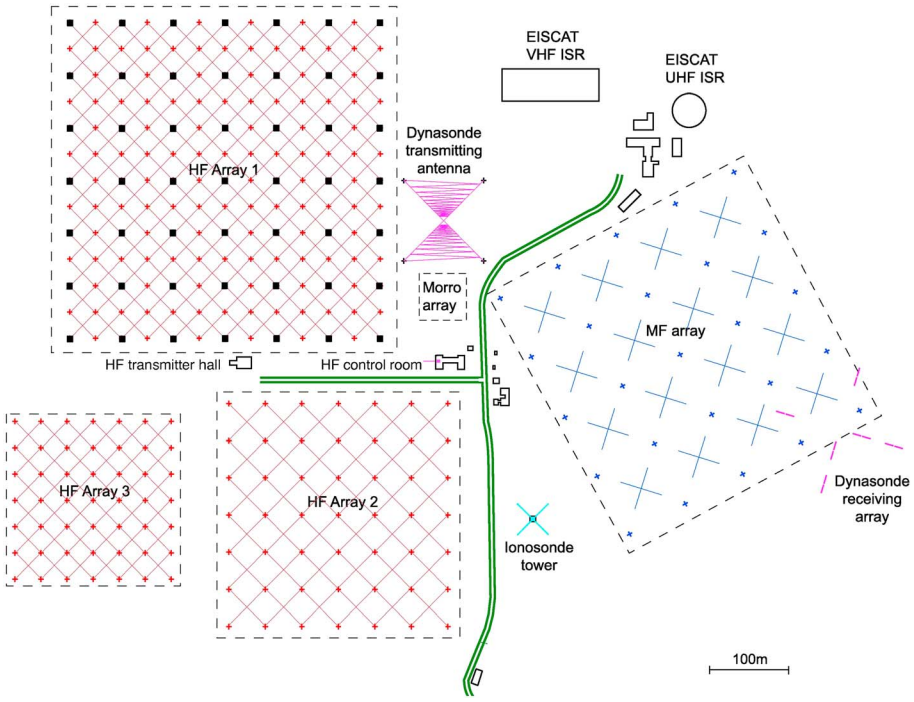

Figure 1. Scale map showing the HF antenna arrays in relation to other radio research infrastructure at Ramfjordmoen. Geographic north is at the top. The red HF arrays of the heating facility show the wooden masts (small crosses) supporting the ends of crossed full-wave dipoles oriented along the diagonals. The small black squares in HF Array 1 mark the original 22 m tall wooden masts from the original low frequency array, which was destroyed in a storm in 1985. The Dynasonde antennas are connected to an HF radar (Dynasonde) located in the HF control room [*Rietveld et al*., 2008]. The EISCAT incoherent scatter radar (ISR) antennas and buildings are shown at the upper right. The large blue crosses show the crossed half-wave dipoles of the 2.78 MHz MF radar transmitting antenna, suspended between masts (small blue crosses). The ionosonde tower supports the transmitting antenna for the University of Tromsø's Digisonde. The Morro array is an antenna for a 56 MHz MST radar from the University of Tromsø. The green double line shows the road, and the unlabeled boxes are buildings or huts with optical and other instruments.

reasons for replacing the old synthesizers were increasing unreliability and the limitations in amplitude and phase control using the old computer hardware [*Rietveld et al*., 1993]. Another advantage of the new exciter units is that they can provide a true zero power output, whereas the previous synthesizers still had a weak residual signal in spite of the 70 dB attenuation provided by a solid-state switch (also called SOUSY switch because it was used to modulate the HF signal in an early MST radar experiment by using the SOUSY radar receiver and radar controller [*Czechowsky et al*., 1983]). This can be important for some experiments like those utilizing the new HF radar capability described later.

The new exciter is now placed in the transmitter building, thus making the long copper cables between the buildings redundant. The control system is split between the control room and transmitter hall with all time-critical connections being brought through optical fibers. There are VMEbus computer crates in the transmitter hall and control room connected by an optical VMEbus link, with the controlling computer in the control room. A GPS-disciplined rubidium oscillator provides the frequency reference for the exciters in the transmitter hall, and a separate GPS-clock provides a frequency reference for the new receiver in the control building as well as the timing synchronization for all transmitter and receiver functions. There is a transmitter radar controller in the transmitter hall and a receiver radar controller in the control room. These are programmable by using commands in a language called TARLAN (Transmitter And Receiver LANguage), which is also used for the EISCAT radars. Radar controller memory allows a maximal size of a compiled TARLAN program to have 256 k instructions. The 38 output bits are clocked at 10 MHz so that all commands are issued with 100 ns granularity. The radar controller timing is determined by a start pulse derived from a GPS-disciplined clock.

Figure 2 is a schematic diagram of essential hardware of the HF facility. RF drive signals for the 12 Heating transmitters T1–T12 are generated by the Heating exciter, which uses direct digital synthesizers to produce the RF carrier frequencies. The exciter is also capable of modulating the carrier by rapidly changing its phase,

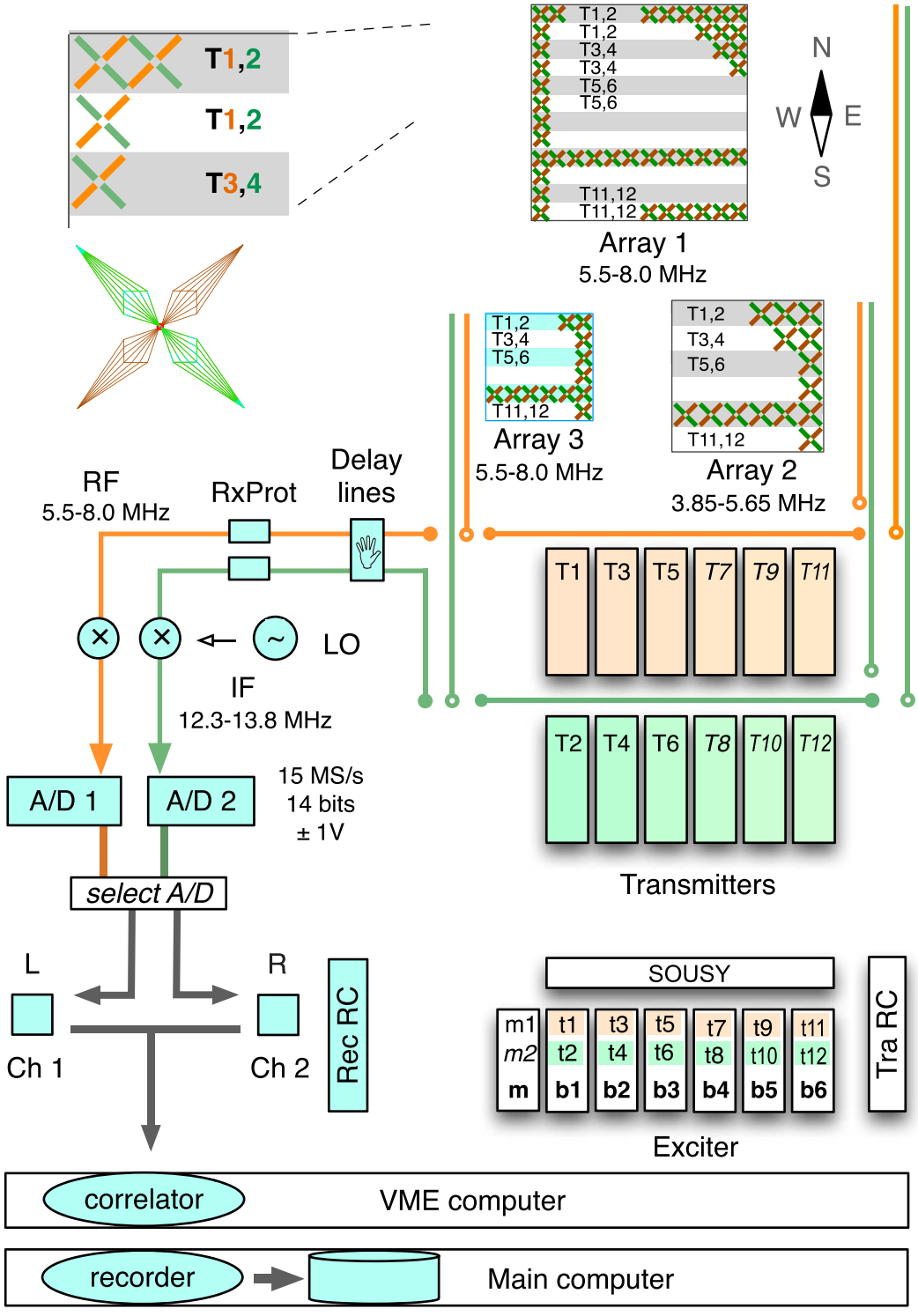

Figure 2. Schematic diagram of the RF generation, transmission lines, antennas, and receiver of the upgraded HF facility. The transmitter radar controller (Tra RC) controls the exciter units and the "SOUSY" switch. Exciter units m1 and m2 provide reference signals for the output phase measurements of transmitters T1–T6 and T7–T12, respectively. The color coding shows the orientation of the antennas connected to the odd and even numbered transmitters, respectively. An expanded view of one stylized crossed dipole antenna illustrates the rhombically broadened layout of the wire elements. Below this at the left is shown the two-channel receiver.

amplitude, and frequency by signals from the radar controller, based on values loaded into the onboard memory. The exciter consists of seven exciter boards (labeled as m and b1–b6 in Figure 2), each housing two AD9953 DDS units each of which features a 14-bit digital to analogue converter. Every exciter board receives a common 10 MHz frequency reference signal, which is derived from a GPS-disciplined rubidium frequency standard (Stanford Research Systems PRS10). For both DDS units on an exciter board there is a 16 kb memory to support flexible changes in one or more of amplitude, frequency, or phase offset. For example, the frequencies can be set by using a 32-bit word which, with the 200 MHz clock internal frequency, gives a frequency resolution of 46.6 mHz. The frequency tuning and control words are loaded into the AD9953 via a serial I/O port. The exciter master board (m) houses the master DDS units m1 and m2. Master unit m1 is used to synchronize all the DDS units in phase, and it also provides a common phase reference to T1–T6 for measuring the output phase. Master unit m2 is used as the common phase reference for T7–T12. This grouping of the master oscillators with the transmitters is reconfigurable by re-cabling, but the chosen grouping is suitable for operation of two groups of transmitters each using the northern and southern half, respectively, of an antenna array with different frequencies.

The exciter boards b1–b6 house the DDS units t1–t12, which provide the RF drive to the power amplifiers T1–T12. The 12 RF drive signals are each routed via a solid-state switch (SOUSY switch), which allows on/off switching for each drive signal and also provides an optional 180° phase flip for each drive signal. Because there are only 12 radar controller bits available to control the 12 SOUSY switches and 12 SOUSY phase-flips, each bit is arranged to operate on two SOUSY switches simultaneously. TARLAN syntax such as "RFON3&4" indicates that one bit controls a pair of transmitters (T3 and T4) feeding a row of antennas, and "FLP1&3" indicates that phases of two transmitters (T1 and T3) connected to two rows with the same orientation can be reversed. The exciter programs are loaded via a serial interface within a few seconds. The timing of the exciter commands and the SOUSY switch is controlled by bits from the transmitter radar controller and can be set with 100 ns granularity. The power-saving feature of the power amplifiers is controlled by the PSAVON bits of the receiver radar controller, where each bit controls the two transmitters connected to one antenna row.

Although the exciters can set the absolute amplitudes and relative phases between the DDS units accurately, it is still necessary at some point to have performed the traditional phasing procedure, whereby the powers are slowly increased as the exciter phases are adjusted to give the desired values at the transmitter outputs for a given frequency, polarization, beam direction, and transmitter combination. This is because the uncertain phase changes through the transmitter and the close coupling between antennas make a purely theoretical setting unpractical. Once performed, however, the final values for each transmitter are stored and can be re-loaded into the exciter memory at will. These loaded values defining a continuously transmitting beam with a given power, polarization, and direction are the basis for modulations of any of these parameters. For example, amplitude modulation of the HF wave is performed by stepping through a list of amplitude values between 1 and 0, where 1 corresponds to the maximum, pre-loaded value.

Frequency stepping is performed by incrementing through a list of frequencies loaded into the exciter memory. Here it is desirable to keep the frequency steps small enough (usually a few kHz to about 20 kHz) such that the automatic tuning and antenna matching circuits in the transmitter can adjust to the new frequency, which is done by variable vacuum capacitors controlled by a phase-locked loop. Phase changes such as for coding a radar transmission pulse can also be made by putting them into a similar list. Results from one of the first frequency stepping experiments using the new exciter are shown in Figure 3.

When performing frequency stepping there should also be a corresponding list of small phase changes so as to keep the beam pointing in exactly the same direction since changing the wavelength (i.e., frequency) alters the array beam pattern if the phase difference between rows stays constant. This has not been done up to now since the frequency changes and hence pointing changes have been very small, but the phase correction is being implemented. These lists of phase, amplitude, and frequency values (in a ".paf" file) are best produced by separate scripts since they tend to be long. Once loaded into the exciter memory, the radar controller program updates the actual values which takes 320 ns/byte + 200 ns per instruction. The shortest dwell time is 1.1 μs if only amplitude or phase is being changed and 3.7 μs if amplitude, frequency, and phase are all being updated.

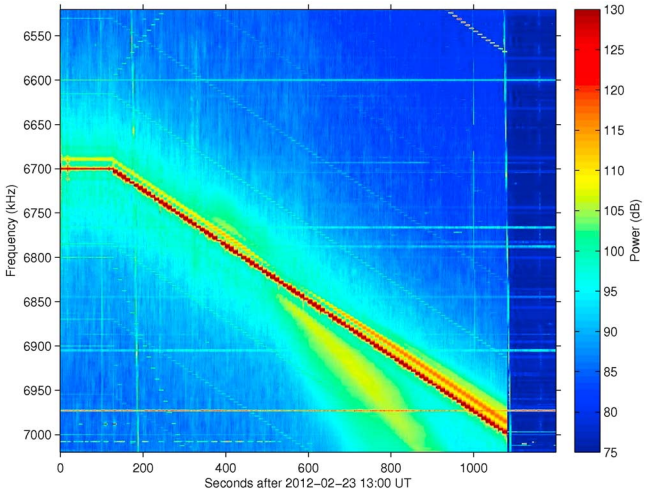

Figure 3. An example of the frequency stepping capability of the new exciter. The spectra of the reflected HF wave and associated stimulated emission sidebands were recorded by a digital sampling receiver 15 km east of the HF facility. The HF carrier was stepped in 3.125 kHz steps every 10 s around the fifth gyroharmonic. Typical SEE features are seen, like the downshifted maximum about 12 kHz below and the broad upshifted maximum increasing in frequency as one steps further above the gyrofrequency, which is at 6.820 MHz at 215 km according to the IGRF model for 2011.

5. Antenna Gains, Effective Radiated Powers, and Ground Conductivity Effects

With the more sophisticated modeling of the heating effects and energy balance calculations attempted in recent years [e.g., *Senior et al.*, 2011; *Bryers et al.*, 2012] the accuracy of the antenna gains and beam shapes becomes increasingly important. The effective radiated power (ERP) in most early publications up to about 1999 was calculated from the following formula for Arrays 2 and 3 and up to October 1985 for Array 1 when it was destroyed in a storm:

$$\mathrm{ERP[MW]} = 360\left(\frac{P}{125}\right)\left(\frac{n}{12}\right)^2$$

Here P is the individual average transmitter power in kW and n is the number of transmitters used (P. Stubbe, private communication). This formula is based on the maximum ERP with a full complement of 12 transmitters each at 125 kW with an average antenna array gain of 23.8 dBi [*Stubbe et al.*, 1982] giving 360 MW. The actual radiated power is proportional to the number of transmitters in use, and the array gain is proportional to the length of a broadside array, which in our case is crudely proportional to the number of transmitters used, which explains the last term. By July 1990 Array 1 had been rebuilt for higher frequencies (5.4–8 MHz) with a higher gain, so for only this array the factor 360 was replaced with 1200 and the divisor 125 became 100. These formulae assume a fixed antenna gain of approximately 24 dBi for the original arrays and approximately 31 dBi for the rebuilt Array 1, for a vertical beam. The divisors 125 and 100 reflect the fact that the planned full power per transmitter was 125 kW but in practice turned out to be 100 kW. In fact, for an array with fixed antenna spacing the gain will vary as a function of frequency by about 3 dB over the frequency range of each array. Clearly, the formula above gives only a rough estimate of the ERP. An assumption used in the estimates is that the ground is a perfect reflector.

Since 2000 the antenna gains were calculated more accurately by using EZNEC (www.eznec.com/). This software package uses the well-known Numerical Electromagnetics Code (NEC), which was developed at the Lawrence Livermore National Laboratory, USA. (http://en.wikipedia.org/wiki/Numerical_Electromagnetics_Code). A model of the antenna arrays was made, whereby each rhombically broadened antenna was approximated by a single wire. The power and phase of each transmitter, which has been logged by computer since 2000, were used to define the voltage source for each antenna in an east-west aligned row. The currents are calculated in each antenna self-consistently, and the radiation pattern is calculated so that the ERP in any given direction can be calculated. More recently, one of us (A. S.) has developed a software package by using open source NEC-2 and GNU Octave running on a Linux platform to calculate beam patterns and ERP from the automatically written transmitter log files in near real time.

An example of the transmitted beam pattern and ERP calculated by using this package for a typical field-aligned experiment using Array 1 is shown in Figure 4. Although the intention in this experiment was to radiate pure O-mode, slightly uneven powers, and slightly inexact phases on the different transmitters caused some X-mode leakage. Such unwanted power in the unwanted polarization can be important in the interpretation of some experimental data, which is why we routinely calculate and plot both polarizations. An example of the beam from Array 2 is shown in Figure 5. Because Array 3 is simply a smaller version of Array 2 it has patterns similar to those of Array 2, whereby the frequency must be scaled up by a factor of $\sqrt{2}$.

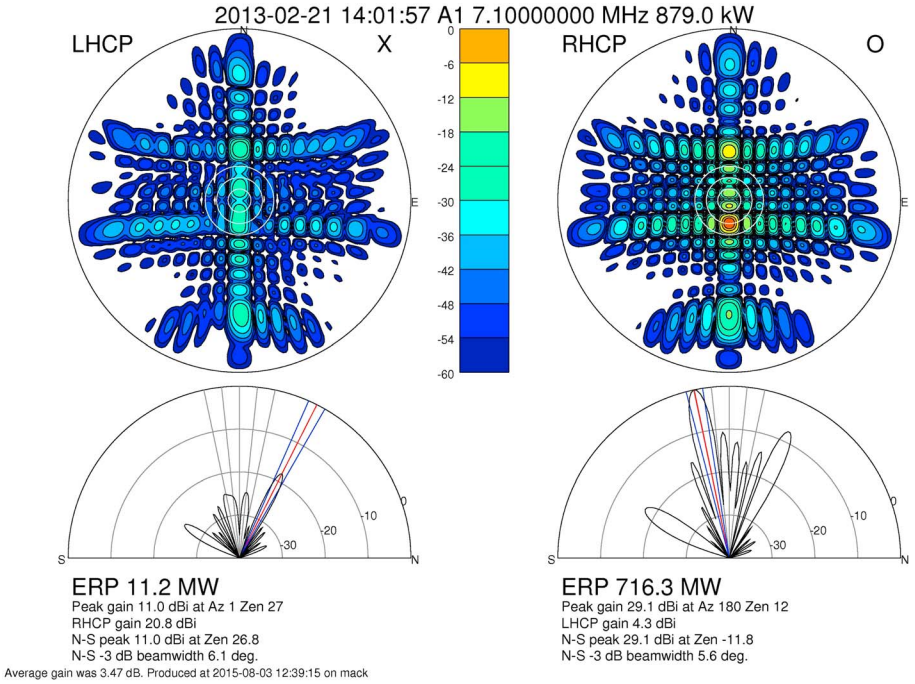

Figure 4. Calculated transmitter beam patterns and effective radiated power (ERP) for the two circularly polarized modes for an experiment at 7.1 MHz using all transmitters on Array 1 for the field-aligned direction. Perfect ground conductivity is assumed.

In all the above modeling, a perfectly conducting ground is assumed but the EISCAT HF facility has no artificial ground plane. In reality, the ground is not a perfect reflector and its conductivity and dielectric constant depend on the material of which it is composed. A seismic and electrical resistivity survey of an area close to the EISCAT site [*Mauring and Tønnesen*, 1990] indicated that the ground is composed of a 0.8–1 m layer of soil overlying a 7.5–10 m layer of dry sand and gravel in turn overlying a 150–160 m layer of saturated fine sediment containing another layer of sand and gravel. Below the fine sediment is rock. The antenna electromagnetic modeling was repeated by using conductivities and dielectric constants typical of the different ground media. The model only allows a single layer of ground material to be included, so it was not possible to make use of the full geological profile. The results indicated that the ERP in the case of the real ground is approximately 75% of that when a perfect ground is assumed. This overestimation of the power may be an important factor to consider in any detailed modeling of heating effects, as the paper by *Senior et al.* [2011] suggests. It would seem that putting down a suitable grid of wires as an artificial ground plane could be a useful investment to improve the effective radiated power significantly, especially as the output of the transmitter tubes decreases with age.

6. Receiver

The HF facility was never intended to operate as a radar, so it never had a receiving capability. There are at least two areas of research that, however, would benefit from a high-power HF radar co-located with the EISCAT incoherent scatter radars. One is to search for magnetospheric echoes, i.e., echoes coming from above the *F* region peak out to perhaps thousands of kilometers, associated with auroral ion-acoustic waves, which have been observed at 224, 500, and 933 MHz [*Rietveld et al.*, 1991; *Sedgemore-Schulthess and St.-Maurice*, 2001; *Schlatter et al.*, 2015]. These have been called Naturally Enhanced Ion Acoustic Lines. It would be interesting to see if related echoes could be seen at the highest heater frequency, 7.953 MHz corresponding to 38 m wave structures, from along the magnetic field line at high altitude. The other area of research is mesospheric echoes, particularly those HF echoes associated with polar mesospheric summer echoes (PMSE) or winter echoes seen by VHF and even UHF radars. Again, the HF radar frequency would be the highest heater frequency but the direction would be vertical.

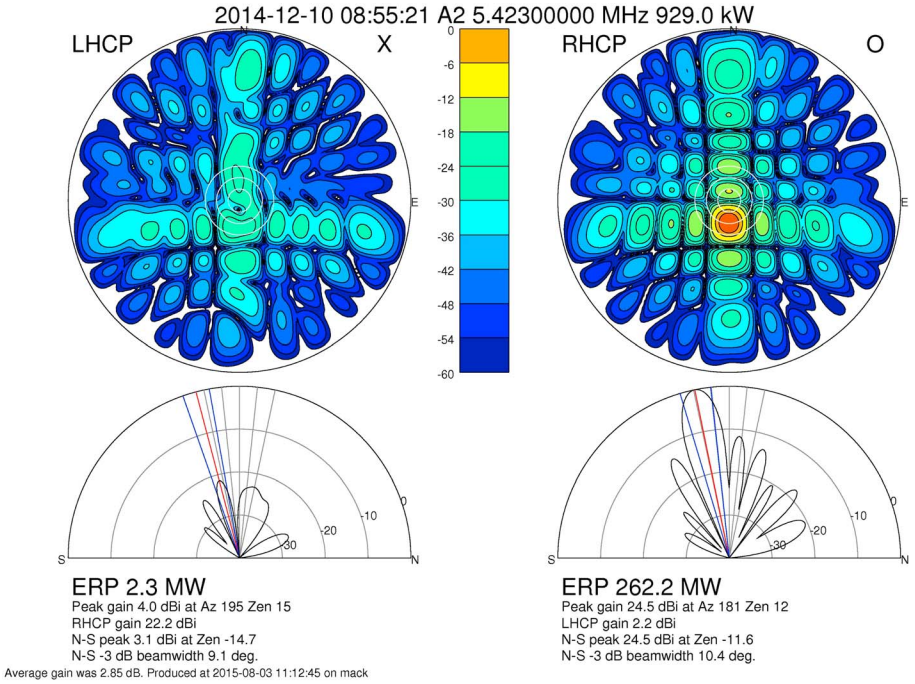

Figure 5. Calculated transmitter beam patterns and effective radiated power (ERP) for the two circularly polarized modes for an experiment at 5.423 MHz using all transmitters on Array 2 for the field-aligned direction. Perfect ground conductivity is assumed. The beam pattern for a frequency of 6.67 MHz on Array 3 is almost identical to this.

Since 1990 we have two arrays (1 and 3) capable of operating between 5.4 and 8 MHz. It was decided to keep Array 1 for transmission only and use the lower gain Array 3 as a receiving antenna by disconnecting the 12 coaxial feeds from the transmitters and combining the signals from each of the six antenna rows with the same alignment into two pairs of signals using the appropriate delay lines for the given frequency and tilt direction (see Figures 1 and 2). These two signal channels, coming from orthogonal sets of antennas, allow discrimination of the polarization. After passing through a receiver protector these signals are amplified, filtered, mixed up in frequency, and sampled at 15 MHz by using two spare EISCAT radar receiver analog to digital computers and two channel boards, similar to the receiver described in Figures 7 and 8 of *Wannberg et al.* [1997] for the Svalbard radar. This setup using two channels of data, with phasing cables cut for vertical reception at 7.953 MHz, has been successfully used for mesospheric research as is described in the results shown later.

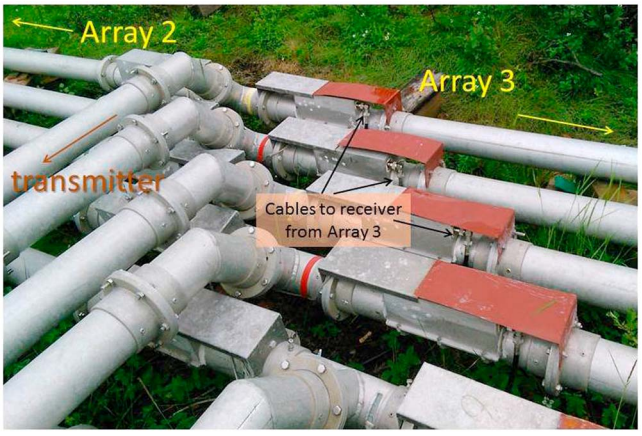

Figure 6. Photo of the coaxial switches, which have been modified such that a connection to Array 3, is made for the receiver whenever the switches are set to Array 2. A set of similar switches located between the transmitters and the switches shown here are used to switch the transmitters to Array 1.

7. Modified Coaxial Switches

A coaxial switch which enables a transmitter to be disconnected from one array and connected to another actually consists of two motor-driven switches, one on each side of a coaxial T-piece coming from the transmitter as shown in Figure 6. One motor moves a short piece of inner conductor tube to make a connection to an array, while the other motor breaks the connection to the other array. In 2013, the coaxial switches shown in Figure 6 were modified to allow an automatic receiver connection to Array 3 whenever those switches connected the coaxial line from the transmitter to Array 2. A spring-loaded contact was made from the coaxial N connector to the inner conductor of the Array 3 aluminum coaxial line whenever the switch was moved to Array 2. Equal length RG213 coaxial cables connected these receiver outputs to a patch panel inside the transmitter building so that phasing cable changes could be made easily inside or connections could be made to the planned HF digital beamformer. The modified coaxial switches now allow an easy transition from transmitter operation on Array 3 to receiver operation and vice versa.

One possible weakness in using Array 3 as a receiving antenna is that some of the many aluminum connectors in the coaxial cables between transmitter and antenna develop poor contacts, which can be seen as an increase in impedance on a time domain reflectometer (TDR). It is thought that a layer of oxide forms at these connectors. When used for high-power transmission these oxide layers are thought to be "burnt through" and the transmissions are unaffected showing a normal standing wave ratio. For passive reception with very weak signals, however, these poor contacts may prevent the signal transfer from some antennas. By having the possibility to transmit as well as receive, with the modified coaxial switches, we were able to test this theory by making a short transmission and comparing the TDR measurement on the receive line after the transmission with that before. The TDR measurement indeed showed that any poor connection in the main line disappeared after the transmissions and this state would usually last for a day or so.

8. EROS Control Software

EROS, which stands for EISCAT Realtime Operating System, is a system of programs and processes based mainly on Tool Command Language (Tcl), and C. EROS was developed to control all the essential units of the ISRs like radar controllers, antennas, and receivers, except the transmitter amplifiers themselves. Since much of the hardware used to upgrade the RF generation were spare EISCAT radar units like the radar controller and digital receiver boards, it was logical to use the same software to control them. There was nevertheless much new hardware like the DDS exciter units and many transmitter functions, which had little or no counterpart in the radar software so that a considerable amount of additional functionality had to be added. A list of Heating specific commands is available at https://www.eiscat.se/groups/Documentation/UserGuides/eros4docs.

Commands can be given to EROS either interactively from a terminal or from script files called "ELAN files," which stands for Experiment LANguage. The time granularity of EROS commands is 0.1 s so that timing of heater modulation signals can often be done from elan scripts, which start and stop various simple radar controller programs. It is not intended or guaranteed, however, that sustained sequences of commands be executed reliably at this rate. For very precise timing, especially on short microsecond or millisecond time scales everything can be programmed in a tlan file, which runs in the radar controller. This timing sequence may be very long (many minutes) and run only once, or it may be very short and repeat many times over. Overall, the flexibility is very high and complex programs can be made either within the radar controller or within the EROS scripts, which control what is run in the radar controllers, or both. The EROS scripts also control when transmitter parameters are measured and logged, which is done on a comparatively slow, seconds, time scale. EROS has built-in functions that can calculate the required relative transmitter phases for a particular beam direction and polarization and can save such beam definitions for future use.

There is a general problem in logging frequencies that are set by the radar controller since they are not measured and not known to the EROS system. The other essential parameters, transmitter power, and phase with respect to a reference synthesizer (which can also be stepped in frequency in synchronism with the transmitter synthesizers) are measured. A program has been written which runs off-line to simulate the radar controller's stepping of frequencies and writes a corrected log file.

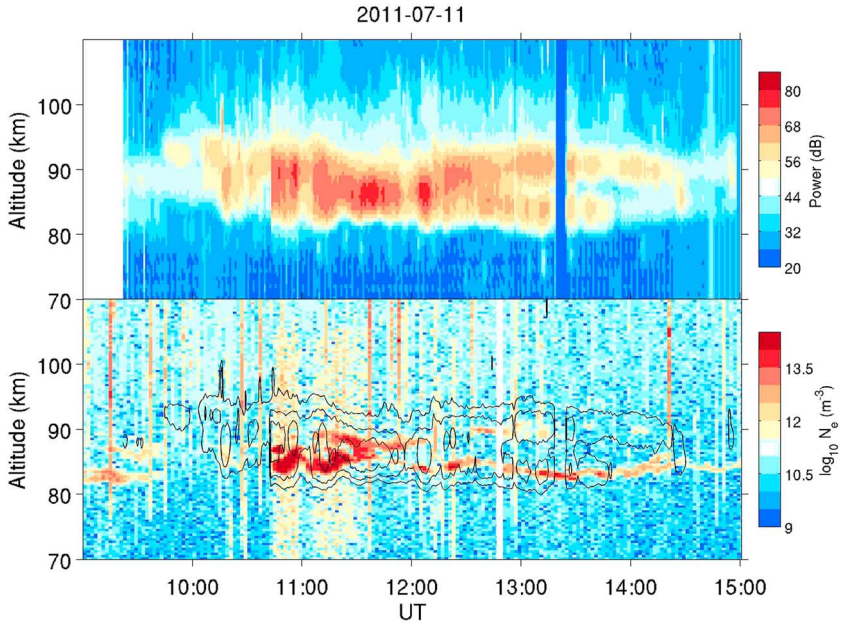

Figure 7. (top) Range-time-power plot of mesospheric echoes at 7.953 MHz. (bottom) Range-time-power plot of mesospheric echoes at 224 MHz, expressed as electron density. Contours of the 7.953 MHz echo power are overlaid.

Extensions to EROS are planned to control the 12 Ettus Universal Software Radio Peripheral (USRP) N200 digital samplers, described later, for use in the new radar mode.

9. High-Power HF Radar Results

9.1. Mesospheric Results

The phenomenon of polar mesosphere summer echoes [*Rapp and Lübken*, 2004] has been studied by using the HF facility to modulate the strength of the echoes observed by the EISCAT VHF radar at 224 MHz. This modulation, a result of electron heating, provides strong confirmation of the idea that PMSE is caused by negatively charged ice particles in the mesopause region [*Havnes et al.*, 2003]. PMSE modulation experiments at EISCAT have usually employed the VHF and UHF radars to observe PMSE. The upgraded HF facility makes it possible to use subsets of transmitters simultaneously for modulating the PMSE and probing it by radar at HF. In July 2011, an experiment was performed during which 10 of the 12 transmitters were operated on 5.423 MHz to modulate PMSE, while the remaining two were operated on 7.953 MHz in radar mode. The heating transmission consisted of a 20 s pulse every 180 s, while the radar transmitted a 40 μs pulse every 10 ms. The HF radar pulse envelope was given a raised-cosine shape by using the amplitude modulation capability of the Heating exciters to control the bandwidth of the transmission and reduce the risk of interference to other HF radio users.

Figure 7 shows an example of the HF radar echoes compared with those obtained from the EISCAT VHF radar. The VHF radar measurements have a range resolution of 360 m compared to the 6 km of the HF radar, and much more fine range structure can be seen in the VHF data. However, there is very good agreement in the general structure of the echoes between the two radars. A notable difference between the two is the behavior of the upper and lower parts of the echo after 13:00 UT. The upper branch remains strong at HF, while the lower branch weakens. At VHF, the reverse is the case. More recent results using a pair of 20 baud complementary codes with 10 μs bauds giving 1.5 km range resolution, showing an HF-heater induced modulation of the HF-radar echoes, were published by *Senior et al.* [2014]. These examples would not have been possible without the upgrades described here.

9.2. Magnetospheric Radar Attempts

An example of an attempt at magnetospheric radar from 01 December 2010 is shown in Figure 8. From 20:18 UT all 12 transmitters at 80 kW each were used at 7.953 MHz on Array 1, phased for O-mode polarization and tilted 18° south of zenith, to transmit a 1 ms uncoded pulse every 40 ms. Reception used Array 3

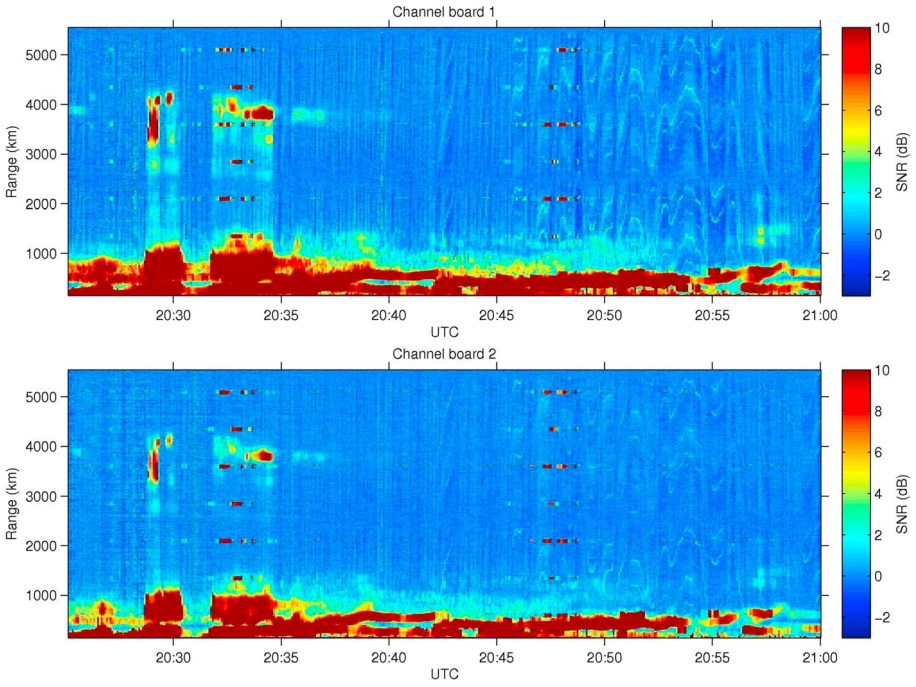

Figure 8. Results from an attempted magnetospheric radar experiment on 01 December 2010. The phasing of the antennas was for a frequency of 7.953 MHz, 18° south of zenith. The transmitting antennas (Array 1) were phased through programming of the exciters, whereas the receiving antennas (Array 3) were phased through fixed-length delay lines. The 1 ms uncoded pulses were transmitted every 40 ms. The Channel board 1 data are from the combined signals of the antennas oriented from north-east to south-west, and the channel board 2 data from the combined signals of the orthogonal antennas.

with the receiver configuration in Figure 2 such that the two channels of echoes in Figure 8 are from the summed signals using the appropriate phase delay lines from each of the two sets of orthogonal antennas. The results shown here are fairly typical, with many echoes below about 1000 km range, some direct interference from local ionospheric sounders (short lines separated by 1500 km every 15 min), and weaker quasi-continuous interfering signals of unknown origin. The echoes at around 1000 km are most likely from ground scatter through antenna sidelobes, as seen in earlier attempts by *Senior et al*. [2008], who also discuss other sources of echoes that are not magnetospheric. A detailed discussion of such echoes as seen by the Super Dual Auroral Radar Network radars and their use in detecting atmospheric gravity waves is given by *Samson et al*. [1990]. The striking echo group around 3000–4000 km is possibly of magnetospheric origin, but their correlation with echoes from ~1000 km suggests that they are also likely to be ground scatter echoes. Without information on the echo direction of arrival it is impossible to confidently identify magnetospheric echoes. This is only one of several reasons to upgrade the receiver to a digital 12-receiver system to enable phase information from the antenna rows to give us the direction of arrival in the north-south plane. This will be described in the next section.

10. Future Directions

At present we are implementing a 12-channel digital acquisition system by using six USRP N200 receivers [www.ettus.com/product/category/USRP-Networked-Series] to directly sample the signals from the six rows of orthogonal antenna pairs in Array 3, before the delay lines in Figure 2, which then become redundant. From such data we should be able to determine the direction of arrival of any radar echoes in the north-south plane. At present the receiver has been used to measure signals from radio sources like Cassiopeia-A, which will help in calibrating the antenna system and receiver. With this radar mode we should also be able to perform more regular API experiments.

One further, relatively straightforward upgrade would be to install a ground plane under one or all of the arrays to improve the ground reflection, which has always assumed to be perfect in the antenna beam and ERP modeling.

10.1. Second Gyroharmonic Transmissions

Originally, Heating was built to transmit from 2.75 MHz to 4.04 MHz on Array 1, which allowed operation at the second gyroharmonic, which is presently 2.75 MHz at 200 km. This capability was lost when that antenna array was rebuilt after a catastrophic storm that destroyed most of the tower feeds on 25 October 1985. Since then, experiments at HAARP have shown that the second gyroharmonic is indeed of special interest in that it produces electron acceleration leading to stronger than normal RF-induced optical emissions [*Mishin et al*., 2016, and references therein]. It would be of great scientific interest to perform such experiments at EISCAT again. The transmitters are capable of transmitting this frequency but none of the antenna arrays are. In Array 1 the 22 m wooden masts that supported the outer ends of the original 6×6 crossed full-wave dipoles still exist and are marked in Figure 1 by black squares. It might be possible to design a simpler array with a limited number of narrowband antennas (say 1 to 3 per transmitter) above the existing antennas, which are at half that height for roughly twice the frequency. The challenge will be in matching the impedance and feeding the high power to the antennas.

10.2. The New EISCAT_3D Radar

With the planned EISCAT_3D radar [*McCrea et al*., 2015] both UHF and VHF incoherent scatter radars at Ramfjordmoen will be replaced by a new phased array tristatic radar at 233 MHz with the transmitter located near Skibotn, about 52 km east south east of Ramfjordmoen. It is envisioned that Heating operation will continue for some time when EISCAT_3D comes on line, presumably after 2020. The geometry is not optimal for some heating experiments, especially since the HF beam cannot be tilted in the east-west plane. For mesospheric heating experiments the EISCAT_3D radar will need to observe at 33° from the zenith, which should just be possible, but at reduced power. It will not be possible to observe with EISCAT_3D along the magnetic field in the heated region. It is not practical to move the present, 36 year old facility nearer Skibotn. So a new HF facility should be built nearer Skibotn if such experiments are desired in the long term.

One of the subarrays of 96 antenna elements for the new radar will be assembled and tested in Ramfjordmoen in the space south of the VHF antenna (see Figure 1). This small radar should be enough to probe HF-induced ion and plasma waves produced by Langmuir and upper hybrid turbulence, similar to the modular UHF ionospheric radar at HAARP [*Mishin et al*., 2016]. This will be a very useful diagnostic to examine field-aligned effects, which has not been possible with the present VHF antenna because it has been restricted to operate only vertical or northward.

11. Conclusions

The 36 year old HF facility, which is still in high demand and scientifically productive, has been upgraded in the areas of RF generation, software control and monitoring, and characterization of the antenna beam pattern and ERP. In particular, fast frequency stepping experiments to investigate gyrofrequency effects in the ionospheric plasma have been drastically improved. A receiver facility has been added to allow high-power HF radar experiments to be performed. New results have been obtained from mesospheric experiments, and hopefully the magnetospheric radar experiments will bear fruit. Further improvements are possible to improve the beam pattern and ERP and to extend the frequency range. A new HF facility should be built near Skibotn to fully exploit the potential of the planned EISCAT_3D radar.

Acknowledgments
We thank the scientists and staff from the former Max Planck Institute fuer Aeronomie (now Max Planck Institute for Solar System Research) for the design and construction of such an excellent HF facility which, over 30 years later, still provides world-class research results. Markku Postila, Gudmund Wannberg, Toivo Iinatti, Lars Göran Vanhainen, Roger Jacobsen, Guttorm Mikalsen, Stian Grande, Erlend Danielsen, and Arild Stenberg (past and present EISCAT staff) made essential contributions to the upgraded HF facility. We thank Ian McCrea and the UK Natural Environment Research Council and their National Centre for Atmospheric Science for funding most of the digital receiver system as a small capital award in 2013/2014 and Juha Vierinen for the help in specifying the system and for software. The data from Figure 3 were from a combined UK-Russian campaign and the data from Figure 7 from a Norwegian-UK campaign. We thank Nataly Blagoveshchenskaya, Mike Kosch, Cesar La Hoz, and Henry Pinedo for their contribution to making these measurements possible. The data in this paper are available from the first author. EISCAT is an international association supported by research organizations in China (CRIRP), Finland (SA), Japan (NIPR and STEL), Norway (NFR), Sweden (VR), and the United Kingdom (NERC)

References

Belikovich, V. V., S. M. Grach, A. N. Karashtin, D. S. Kotik, and Y. V. Tokarev (2007), The "SURA" facility: Study of the atmosphere and space (a review) [in English], *Radiophys. Quantum Electron.*, *50*(7), 497–526.

Biebricher, A., and O. Havnes (2012), Non-equilibrium modeling of the PMSE Overshoot Effect revisited: A comprehensive study, *J. Plasma Phys.*, *78*(3), 303–319, doi:10.1017/S0022377812000141.

Blagoveshchenskaya, N. F., T. D. Borisova, T. K. Yeoman, I. Häggström, and A. S. Kalishin (2015), Modification of the high latitude ionosphere *F* region by X-mode powerful HF radiowaves: Experimental results from multi-instrument diagnostics, *J. Atmos. Sol.-Terr. Phys.*, *135*, 50–63, doi:10.1016/j.jastp.2015.10.009.

Bryers, C. J., M. J. Kosch, A. Senior, M. T. Rietveld, and T. K. Yeoman (2012), EISCAT observations of pump-enhanced plasma temperature and optical emission excitation rate as a function of power flux, *J. Geophys. Res.*, *117*, A09301, doi:10.1029/2012JA017897.

Chilson, P. B., E. Belova, M. T. Rietveld, S. Kirkwood, and U.-P. Hoppe (2000), First artificially induced modulation of PMSE using the EISCAT heating facility, *Geophys. Res. Lett.*, *27*(23), 3801–3804, doi:10.1029/2000GL011897.

Czechowsky, P., G. Schmidt, and H. Kopka (1983), Medium frequency radar observations in the middle atmosphere, *J. Atmos. Terr. Phys.*, *45*(10), 729–732.

Havnes, O., C. La Hoz, L. I. Naesheim, and M. T. Rietveld (2003), First observations of the PMSE overshoot effect and its use for investigating the conditions in the summer mesosphere, *Geophys Res. Lett.*, *30*(23), 2229, doi:10.1029/2003GL018429.
Kalogerakis, K. S., T. G. Slanger, E. A. Kendall, T. R. Pedersen, M. J. Kosch, B. Gustavsson, and M. T. Rietveld (2009), Remote Oxygen Sensing by Ionospheric Excitation (ROSIE), *Ann. Geophys.*, *27*, 2183–2189.
Kosch, M. J., T. Pedersen, M. T. Rietveld, B. Gustavsson, S. M. Grach, and T. Hagfors (2007), Artificial optical emissions in the high-latitude thermosphere induced by powerful radio waves: An observational review, *Adv. Space Res.*, *40*, 365–376, doi:10.1016/j.asr.2007.02.061.
Kosch, M. J., Y. Ogawa, M. T. Rietveld, S. Nozawa, and R. Fujii (2010), An analysis of pump-induced artificial ionospheric ion upwelling at EISCAT, *J. Geophys.*, *115*, A12317, doi:10.1029/2010JA015854.
Kosch, M. J., C. Bryers, M. T. Rietveld, T. K. Yeoman, and Y. Ogawa (2014), Aspect angle sensitivity of pump-induced optical emissions at EISCAT, *Earth Planets Space*, *66*, 159, doi:10.1186/s40623-014-0159-x.
Kosch, M., M. T. Rietveld, T. Hagfors, and T. B. Leyser (2000), High-latitude HF-induced airglow displaced equatorwards of the pump beam, *Geophys. Res. Lett.*, *27*(17), 2817–2820, doi:10.1029/2000GL003754.
Leyser, T. B. (2001), Stimulated electromagnetic emissions by high frequency electromagnetic pumping of the ionospheric plasma, *Space Sci. Rev.*, *98*, 223–328.
Leyser, T. B., and A. Y. Wong (2009), Powerful electromagnetic waves for active environmental research in geospace, *Rev. Geophys.*, *47*, RG1001, doi:10.1029/2007RG000235.
Leyser, T. B., B. Thidé, H. Derblom, Å. Hedberg, B. Lundborg, P. Stubbe, and H. Kopka (1989), Stimulated electromagnetic emission near electron cyclotron harmonics in the ionosphere, *Phys. Rev. Lett.*, *63*(11), 1145–1147.
Mahmoudian, A., W. A. Scales, M. J. Kosch, A. Senior, and M. Rietveld (2011), Dusty space plasma diagnosis using temporal behavior of polar mesospheric summer echoes during active modification, *Ann. Geophys.*, *29*, 2169–2179, doi:10.5194/angeo-29-2169-2011.
Mauring, E., and J. F. Tønnesen (1990), Refraksjonsseismiske og elektriske målinger ved Ramfjordmoen og Hanslarsanes, Tromsø, Troms Rapp. Nor. Geol. Unders., 90.018.
McCrea, I., et al. (2015), The science case for the EISCAT_3D radar, *Prog. Earth Planet. Sci.*, *2*, 21, doi:10.1186/s40645-015-0051-8.
Mishin, E., B. Watkins, N. Lehtinen, B. Eliasson, T. Pedersen, and S. Grach (2016), Artificial ionospheric layers driven by high-frequency radiowaves: An assessment, *J. Geophys. Res. Space Physics*, *121*, 3497–3524, doi:10.1002/2015JA021823.
Pedersen, T. R., and H. C. Carlson (2001), First observations of HF heater produced airglow at the High Frequency Active Auroral Research Program facility: Thermal excitation and spatial structuring, *Radio Sci.*, *36*(5), 1013–1026, doi:10.1029/2000RS002399.
Rapp, M., and F.-J. Lübken (2004), Polar mesosphere summer echoes (PMSE): Review of observations and current understanding, *Atmos. Chem. Phys.*, *4*, 2601–2633.
Rietveld, M. T., and N. P. Goncharov (1998), Artificial periodic irregularities from the Tromsø Heating facility, *Adv. Space Res.*, *21*(5), 693–696.
Rietveld, M. T., P. N. Collis, and J.-P. St.-Maurice (1991), Naturally enhanced ion-acoustic waves in the auroral ionosphere observed by the EISCAT 933 MHz radar, *J. Geophys. Res.*, *96*, 19,291–19,305, doi:10.1029/91JA01188.
Rietveld, M. T., H. Kohl, H. Kopka, and P. Stubbe (1993), Introduction to ionospheric heating at Tromsø. Experimental overview, *J. Atmos. Terr. Phys.*, *55*, 577–599.
Rietveld, M. T., E. Turunen, H. Matveinen, N. P. Goncharov, and P. Pollari (1996), Artificial periodic irregularities in the auroral ionosphere, *Ann. Geophys.*, *14*, 1437–1453.
Rietveld, M. T., B. Isham, H. Kohl, C. La Hoz, and T. Hagfors (2000), Measurements of HF-enhanced plasma and ion lines at EISCAT with high altitude resolution, *J. Geophys. Res.*, *105*(A4), 7429–7439, doi:10.1029/1999JA900476.
Rietveld, M. T., M. J. Kosch, N. F. Blagoveshchenskaya, V. A. Kornienko, T. B. Leyser, and T. K. Yeoman (2003), Ionospheric electron heating, optical emissions and striations induced by powerful HF radio waves at high latitudes: Aspect angle dependence, *J. Geophys. Res.*, *108*(A4), 1141, doi:10.1029/2002JA009543.
Rietveld, M. T., M. J. Kosch, N. F. Blagoveschchenskaya, V. A. Kornienko, T. B. Leyser, and T. K. Yeoman (2004), Correction to 'Ionospheric electron heating, optical emissions and striations induced by powerful HF radio waves at high latitudes', *J. Geophys. Res.*, *109*, A040306, doi:10.1029/2004JA010460.
Rietveld, M. T., J. W. Wright, N. Zabotin, and M. L. V. Pitteway (2008), The Tromsø Dynasonde, *Polar Sci.*, *2*(1), 55–71, doi:10.1016/j.polar.2008.02.001.
Samson, J. C., R. A. Greenwald, J. M. Ruohoniemi, A. Frey, and K. B. Baker (1990), Goose Bay radar observations of Earth-reflected gravity waves in the high-latitude ionosphere, *J. Geophys. Res.*, *95*, 7693–7709, doi:10.1029/JA095iA06p07693.
Schlatter, N. M., V. Belyey, B. Gustavsson, N. Ivchenko, D. Whiter, H. Dahlgren, S. Tuttle, and T. Grydeland (2015), Auroral ion acoustic wave enhancement observed with a radar interferometer system, *Ann. Geophys.*, *33*, 837–844, doi:10.5194/angeo-33-837-2015.
Sedgemore-Schulthess, K. J. F., and J.-P. St.-Maurice (2001), Naturally enhanced ion-acoustic spectra and their interpretation, *Surv. Geophys.*, *22*, 55–92.
Senior, A., F. Honary, P. J. Chapman, M. T. Rietveld, T. S. Kelso, and M. J. Kosch (2008), High-frequency magnetospheric sounding at EISCAT: Some trials and their implications, *Radio Sci.*, *43*, RS4009, doi:10.1029/2007RS003779.
Senior, A., M. T. Rietveld, F. Honary, W. Singer, and M. J. Kosch (2011), Measurements and modelling of cosmic noise absorption changes due to radio heating of the D-region ionosphere, *J. Geophys. Res.*, *116*, A04310, doi:10.1029/2010JA016189.
Senior, A., M. T. Rietveld, I. Häggström, and M. J. Kosch (2013), Radio-induced incoherent scatter ion line enhancements with wide altitude extents in the high-latitude ionosphere, *Geophys. Res. Lett.*, *40*, 1669–1674, doi:10.1002/grl.50272.
Senior, A., A. Mahmoudian, H. Pinedo, C. La Hoz, M. T. Rietveld, W. A. Scales, and M. J. Kosch (2014), First modulation of high-frequency polar mesospheric summer echoes by radio heating of the ionosphere, *Geophys. Res. Lett.*, *41*, 5347–5353, doi:10.1002/2014GL060703.
Stubbe, P., and H. Kopka (1979), Ionospheric modification experiments in northern Scandinavia—A description of the Heating project Report MPAE-W-02-79-04, Max-Planck-Institut für Aeronomie, Katlenburg-Lindau-FRG.
Stubbe, P., et al. (1982), Ionospheric modification experiments in northern Scandinavia, *J. Atmos. Terr. Phys.*, *44*(12), 1025–1041.
Stubbe, P., H. Kopka, B. Thidé, and H. Derblom (1984), Stimulated electromagnetic emission: A new technique to study the parametric decay instability in the ionosphere, *J. Geophys. Res.*, *89*(A9), 7523–7536, doi:10.1029/JA089iA09p07523.
Thidé, B., H. Kopka, and P. Stubbe (1982), Observations of stimulated scattering of a strong high-frequency wave in the ionosphere, *Phys. Rev. Lett.*, *49*(21), 1561–1564.
Vierinen, J., A. Kero, and M. T. Rietveld (2013), High latitude artificial periodic irregularity observations with the upgraded EISCAT heating facility, *J. Atmos. Sol.-Terr. Phys.*, *105-106*, 253–261.
Wannberg, U. G., et al. (1997), The EISCAT Svalbard radar, a case study in modern incoherent scatter radar system design, *Radio Sci.*, *32*, 2283–2307, doi:10.1029/97RS01803.